Journal of Materials Chemistry C

A study of the doping process in $Li_4Ti_5O_{12}$ and TiO_2 battery electrode materials studied in ion-gated transistor configuration

Journal:	*Journal of Materials Chemistry C*
Manuscript ID	TC-ART-09-2023-003517.R1
Article Type:	Paper
Date Submitted by the Author:	29-Nov-2023
Complete List of Authors:	Garza, José ; Polytechnique Montréal, Engineering Physics Department Camargo, Luan; Polytechnique Montréal, Engineering Physics Department; State University of Londrina, Chemistry Department Karimi Azari, Ramin; Polytechnique Montréal, Engineering Physics Department Neres, Lariel ; São Paulo State University - Araraquara Campus, Instiute of Chemistry; Polytechnique Montréal, Engineering Physics Department Khaleel, Shahid; Polytechnique Montréal, Engineering Physics Department Barbosa, Martin; Federal University of Goias, Institute of Chemistry Soavi, Francesca; Università di Bologna, Department of Chemistry "Giacomo Ciamician" Santato, Clara; Polytechnique Montréal, Engineering Physics Department

ARTICLE

A study of the doping process in $Li_4Ti_5O_{12}$ and TiO_2 battery electrode materials studied in ion-gated transistor configuration

Received 00th January 20xx,
Accepted 00th January 20xx

DOI: 10.1039/x0xx00000x

José Ramón Herrera Garza[a,#], Luan Pereira Camargo[a,b,#], Ramin Karimi Azari[a#], Lariel Chagas da Silva Neres[a,c], Shahid Khaleel[a], Martin Schwellberger Barbosa[d*], Francesca Soavi[e*], Clara Santato[a*]

Understanding how the electronic conductivity of metal oxides used as electrode materials in Li-ion batteries (LIBs) evolves as a function of the degree of lithiation/delithiation is relevant to try to prolong the battery lifetime, which affects, among others, the sustainability of LIBs. We propose the use of ion-gated transistors (IGTs) employing as transistor channel materials films of $Li_4Ti_5O_{12}$ (LTO) and TiO_2 interfaced to the ionic liquid 1-Ethyl-3-methylimidazolium bis(trifluoromethylsulfonyl)imide ([EMIM][TFSI]) including the salt LiTFSI, to study the evolution of the doping mechanism, charge carrier density and mobility with the advancement of lithiation/delithiation in the films. The process of lithiation/delithiation is controlled by the electrical bias applied at the gate electrode, made of carbon paper coated with high surface area activated carbon. The sweeping rate of the gate bias affects the kinetics of Li intercalation/deintercalation and, consequently, the electronic doping of the transistor channel. We discuss how different doping mechanisms, namely electrostatic, "purely" electrochemical, or electrochemical possibly associated to structural changes in the transistor channel are possible for the metal oxide films. We consider such discussion relevant to contribute to the optimal use of the electrode materials in LIBs.

Introduction

In ion-gated transistors (IGTs), the electronic conductivity of the semiconducting transistor channel is modulated by the redistribution of the ions of the ion gating medium at the interface and within the channel. Such redistribution is triggered upon application of an electrical bias at the gate electrode immersed in the gating medium in contact with the channel. IGTs are relevant for flexible and printable electronics, chemo- and bio-sensing and neuromorphic computing.[1,2]

Recently, we proposed IGTs as *in operando* tools to monitor the changes in the electronic conductivity of lithium-ion battery (LIB) cathode materials with the degree of lithiation/de-lithiation of the material. To this purpose, we employed LIB cathode materials as transistor channels. We observed changes in the electronic conductivity, disentangled from ionic conductivity, of $LiNi_{0.5}Mn_{0.3}Co_{0.2}O_2$ (NMC532)- and $LiNi_{1.5}Mn_{0.5}O_4$ (LNMO)-based cathode materials with the degree of delithiation.[3]

In the field of LIBs, lithium titanate ($Li_4Ti_5O_{12}$, LTO) has been considered as anode material (specific capacity 175 mA h g^{-1}).[4,5] It features *zero-strain* upon Li^+ insertion, since the spinel structure of LTO undergoes a transition to the $Li_7Ti_5O_{12}$ rock-salt structure with minimum expansion; the formation of its Solid-Electrolyte-Interphases (SEIs) is object of investigations.[6–8] LTO has a conductivity as low as 10^{-13} - 10^{-8} S cm^{-1}, whereas the conductivity of $Li_7Ti_5O_{12}$, obtained upon lithiation from LTO, ranges between 10^{-2} - 2 S cm^{-1}.[9] Structural and chemical changes in LTO with lithiation/delithiation have been carried out *in situ* by X-ray diffraction (XRD) combined with either *in situ* Bragg coherent diffraction imaging[10] or *in situ* X-ray absorption spectroscopy (XAS).[11,12] Further, *in situ* transmission electron microscopy (TEM) was used in combination with Electron Energy Loss Spectroscopy (TEM-EELS).[13]

[a] Engineering Physics Department, Polytechnique Montreal, Montreal, H3C 3A7, QC, Canada.
[b] Chemistry Department, CCE, State University of Londrina (UEL), Londrina, 86057-970, PR, Brazil.
[c] Institute of Chemistry, São Paulo State University (UNESP), 14801-970, Araraquara, SP, Brazil.
[d] Institute of Chemistry, Federal University of Goias (UFG), Av. Esperança, s/n—Chácaras de Recreio Samambaia, Goiânia, GO 74690-900, Brazil.
[e] Department of Chemistry "Giacomo Ciamician", Alma Mater Studiorum Universitá di Bologna, Via Selmi 2, 40126, Bologna, Italy,
* Corresponding authors: Clara.santato@polymtl.ca, francesca.soavi@unibo.it, martin_barbosa@ufg.br
#These authors equally contributed.
Electronic Supplementary Information (ESI) available: [details of any supplementary information available should be included here]. See DOI: 10.1039/x0xx00000x

TiO_2, due to its abundance, safe operation, and theoretical specific capacity (335 mA h g^{-1}), is a promising alternative for LIB anodes;[14,15] However, it features low charge/discharge rate, related to slow Li^+ insertion kinetics and low electronic conductivity.[16–18] In TiO_2 anatase, upon lithiation, two orthorhombic phases can form, namely $Li_{0.5}TiO_2$ and $LiTiO_2$,[19,20] as observed by *in situ* XRD and TEM.[21,22] The effect of the lithiation degree on the electronic properties has been investigated by *in situ* spectroscopy,[23,24] computational methods and direct conductivity measurements in IGTs.[25,26] Values of the conductivity of 0.4 S cm^{-1} and 0.75 S cm^{-1} have been reported for $Li_{0.5}TiO_2$ and $LiTiO_2$, respectively.[27]

The low electronic conductivity of LTO and TiO_2 has been addressed with several strategies such as creating controlled nanostructures or adding conductive components to the formulation of the electrode materials.[5,28]

In this work, we initially studied in IGT configuration films of an LTO-based anode composite material including a conductive carbon additive (indicated from now on as LTO+C) interfaced to an ionic liquid ion gating medium possibly including Li^+, with the aim to observe changes in electronic charge carrier density and charge carrier mobility in this material as a function of the applied potential and its sweeping rate. The sweeping rate affects the kinetic response of the electrodes, which is principally limited by lithium-ion diffusion and redistribution at the electrode/electrolyte interface and in the intercalation sites of the electrodes, in turn affecting the effectiveness of the bias to trigger the doping. Afterwards, analogous studies were carried out on LTO without carbon additive and TiO_2 films to better understand the fundamentals of Li^+ intercalation and electronic doping in titanium dioxide and double oxide materials, in IGT configuration. Prior to their transistor characterization, films were characterized for their electrochemical behavior, by cyclic voltammetry, and structure, by scanning electron microscopy and X-ray diffraction.

Experimental

Fabrication of Au electrodes on SiO_2/Si substrates

Drain and source Au/Ti electrodes were patterned on SiO_2/Si wafers by subtractive photolithography (lift off process) and deposited by e-beam evaporation. The thickness of the electrodes was 65 nm (10 nm of Ti as adhesion layer, 55 nm of Au). Devices had a channel width of 4 mm and a channel length of 10 µm (Fig. S1).

$Li_4Ti_5O_{12}$ (LTO) and LTO+C films

Lithium titanate films ($Li_4Ti_5O_{12}$, Sigma Aldrich, battery grade 99.5% purity) with and without conductive carbon additive (indicated as LTO+C and LTO) were studied as transistor channel materials. Films were deposited over microfabricated Au on SiO_2/Si substrates by drop-casting. The precursor ink was prepared from LTO and poly(vinylidenefluoride) binder (PVDF, Kynar, 99.5% purity) with a weight ratio of 9:1, in N-methyl-pyrrolidone (NMP, Sigma-Aldrich, 99.5% purity). The precursor ink including conductive carbon (Super P® conductive carbon black, Imerys) was prepared with an 8:1:1 weight ratio of LTO, PVDF, and conductive carbon. For film deposition, the ink was drop-casted onto pre-cleaned substrates and dried overnight in a vacuum oven, at 60 °C. The thickness of the films was 6±1 µm, for both LTO and LTO+C, as measured by profilometry.

TiO_2 films

We prepared a suspension of 0.5 g of Titanium (IV) oxide (Aeroxide® P25, Sigma Aldrich, ≥ 99.5% purity) and 0.2 g of PVDF (Sigma-Aldrich, 99.5% purity) in 10 mL of N,N-dimethylformamide (Acros Organics, 99.8% purity).[29] The suspension was vigorously stirred for 1 hour. We deposited the films by spin-coating (40 µL, 4000 rpm for 40 s). Films were air dried for 30 min at 25 °C, vacuum dried for 40 min at 100 °C, and then treated for 1 h at 450 °C, in a tubular furnace. The thickness of the TiO_2 films was 2.4±1 µm.

Fabrication of carbon paper gate electrodes

For the reference/counter and gate electrodes, we used carbon paper (Spectracarb 2050 A) coated with an ink including high surface area activated carbon (Picactif supercap BP10, Pica) and 20% w/w PVDF binder in NMP. After coating, the electrode was thermally treated at 80 °C overnight.[30] The resulting mass loading of activated carbon in the coating was ca 1 mg cm^{-2}. For the activated carbon electrode potential we used 0 V vs. activated carbon ≈ 3 V vs. Li^+/Li.[31]

Ion gating medium

The ionic liquid 1-Ethyl-3-methylimidazolium bis(trifluoromethylsulfonyl)imide, ([EMIM][TFSI], Iolitec, 99% purity) was purified overnight at 60 °C under vacuum conditions. To gate in presence of Li^+, bis(trifluoromethane)-sulfonimide lithium salt

(LiTFSI, Sigma-Aldrich, 99.95% purity) was dissolved in purified [EMIM][TFSI] to reach a concentration of 0.1 mol L^{-1} in Li^+.

Device assembly

IGTs with TiO_2, LTO, and LTO+C as channel materials were assembled in a N_2 glovebox (H_2O, O_2 concentrations below 3 ppm). We placed a Durapore® PVDF membrane (4 mm × 9 mm, 125 µm-thick) soaked with either [EMIM][TFSI] or [EMIM][TFSI] including 0.1 mol L^{-1} [LiTFSI] in correspondence of the transistor channel. We completed the assembly by placing the reference/counter or gate electrodes (6 mm × 3 mm, 170 µm-thick) on top of the membrane (Fig. S1).

Materials characterization

The thickness of the films was measured using a profilometer (Dektak 150). Two samples for each material were characterized, with eight measurements each sample. The morphological characteristics of the films were studied by scanning electron microscopy (SEM, model: JEOL JSM-7600F), at an accelerating potential of 10 kV. The structure of LTO and TiO_2 films was investigated using X-ray diffraction (XRD, model: Bruker D8), using a Cu-K_α source (wavelength 1.54 Å).

Electrical and electrochemical characterizations

Electrical and electrochemical characterizations were performed in an N_2 glovebox (H_2O, O_2 concentrations below 3 ppm). Cyclic voltammetry measurements were performed using a VersaSTAT4 potentiostat. Transistor characteristics were measured in a home-made electrical probe station using an Agilent B1500A semiconductor parameter analyzer. The same transistors were investigated in [EMIM][TFSI] and, afterwards, in [EMIM][TFSI] including LiTFSI.

Results and Discussion

Structural and morphological characterizations

We initially collected the SEM images of TiO_2, LTO, and LTO+C films to confirm their porous nanostructure (Fig. 1).[29,32–35] We also studied the films by XRD (Fig. S2 (a-c)). The TiO_2 pattern exhibits peaks corresponding to the anatase (Joint Committee on Powder Diffraction Standards, JCPDS#1-083-2243: 25.3° (101), 37.0° (103), 37.9° (004), 48.1° (200), 53.9° (105), 55.1° (211), 62.8° (204)) and rutile (JCPDS#00-034-0180: 27.5° (110), 36.1° (101), 54.4° (211), 56.7° (220)) phases (Fig. S2 (a)).[32,33] The patterns of LTO and LTO+C films showed diffraction peaks

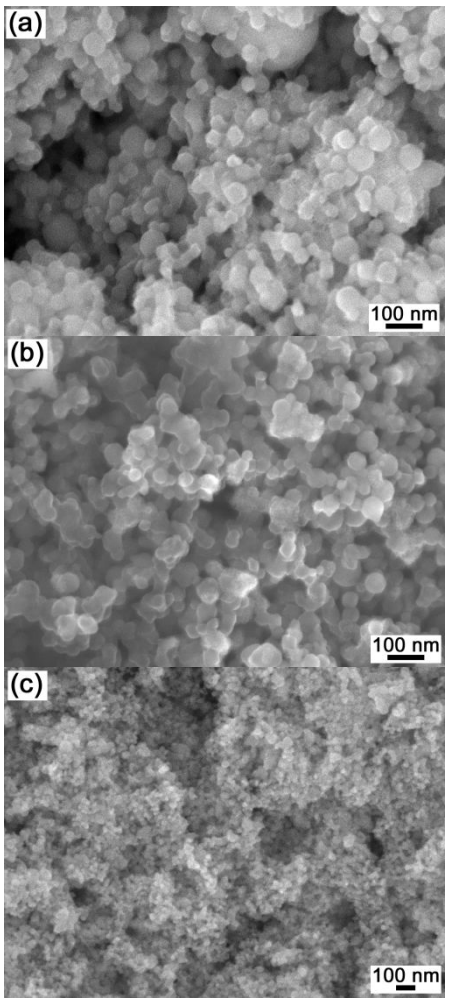

Fig. 1 Scanning electron microscopy images of films of LTO (a), LTO+C (b), and TiO_2 (c), deposited on a SiO_2/Si substrate.

indexed to spinel structure characteristic of $Li_4Ti_5O_{12}$ (Fd3m space group). Indeed, the peaks at 18.3° (111), 35.6° (311), 43.3° (400), 47.4° (331), 57.2° (333), 62.8° (440), and 66.0° (531) belong to the LTO structure (JCPDS#00-049-0207) (Fig. S2 (b-c)).[34,35] The addition of carbon did not influence the spinel structure.

Electrochemical response and IGT characteristics of LTO and LTO+C films

Initially, we ran the cyclic voltammograms of LTO and LTO+C films in IGT configuration. Here, the metal oxide films, included between source and drain contacts, were used as the working electrode and a high surface area carbon electrode acted as the counter and reference electrodes (short circuited). The cyclic voltammograms for LTO obtained at 0.5 and 1 mVs^{-1} feature a broad reduction signal between -2.25 V and -2.5 V *vs*. activated carbon, during the cathodic sweep, and two oxidation signals,

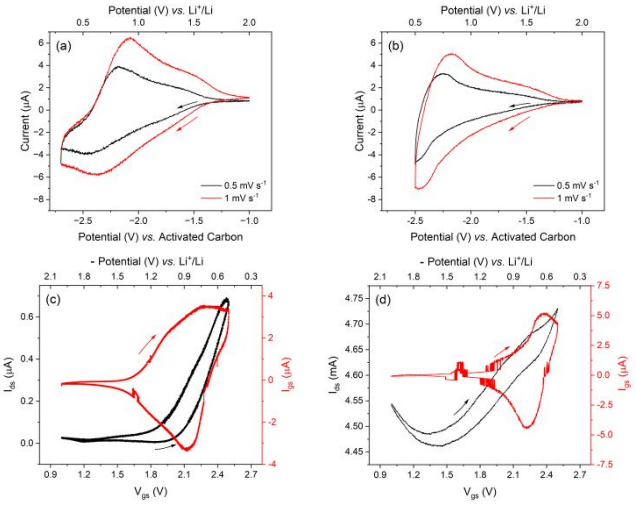

Fig. 2 Electrochemical and transistor characteristics of LTO (a, c) and LTO+C (b, d) films. Cyclic voltammograms of (a) LTO, (b) LTO+C. Transfer characteristics of (c) LTO and (d) LTO+C, at V_{gs} sweep rate of 1 mV s^{-1}, V_{ds} = 1 V. Ion gating medium: 0.1 mol L^{-1} LiTFSI in [EMIM][TFSI].

between -2.25 V and -1.8 V and -1.65 V and -1.25 V (shoulder), during the anodic sweep (Fig. 2 (a), Fig. S3). These features are attributed to the redox activity of the Ti^{3+}/Ti^{4+} couple.[36] With LTO+C films, the cathodic current features an inflection point at about -2.25 V, likely associated to the beginning of a voltammetric signal (we reversed the scan at -2.5 V to ensure the stability of the system); the oxidation signals are analogous to those of LTO (Fig. 2 (b)).

For IGTs based on LTO films, the transfer characteristics (drain-source current (I_{ds}) *vs.* gate-source voltage (V_{gs}) at constant drain-source voltage (V_{ds})) show that I_{ds} increases slightly from V_{gs}=1.9 V and then more significantly from V_{gs}=2.1 V (Fig. 2 (c), Fig. S4, Fig. S7, Table S1). I_{ds} shows lower values during the forward scan with respect to the backward one (counterclockwise hysteresis), likely due to the slow diffusion of the lithium cations in the channel.

For LTO+C, the transfer characteristics show that I_{ds} decreases from V_{gs}=1 V to 1.35 V; for V_{gs} > 1.35 V, I_{ds} increases (Fig. 2 (d), Fig. S5, Fig. S7, Table S1). I_{ds} for LTO+C curve shows higher I_{ds} values during the forward scan with respect to the reverse scan (clockwise hysteresis). The difference in the type of hysteresis (anti-clockwise for LTO and clockwise for LTO+C) is attributable, among others, to the faster lithiation process in the highly conductive LTO+C films, compared to LTO counterparts.

Despite I_{ds} being about four orders of magnitude higher for LTO+C than LTO (due to the presence of the conductive carbon additive), I_{gs} has the same order of magnitude for the two cases. This shows the difference between the processes that determine the values of I_{ds} (predominant electronic transport in the oxide and/or in the composite of the oxide with the carbon conductive additive) and I_{gs} (ion accumulation at the gate electrode).

From the transfer characteristics, we deduced the charge carrier density, n, as $n = \frac{Q}{eA} = \frac{(\int I_{gs} dV_{gs})}{r_v e A}$ where Q is the charge accumulated during the forward scan (obtained through the integration of I_{gs} *vs.* time), A is the geometric area of the film exposed to the ion gating medium (4×10^{-2} cm^2), r_v is the V_{gs} scan rate, and e is the elementary charge.[37] The charge carrier mobility, μ, was obtained through $\mu = \frac{L}{W n e} \frac{I_{ds}}{V_{ds}}$ where L is the source-drain interelectrode distance (10 μm) and W is the electrode width (4 mm).

For LTO, at 1 mV s^{-1}, Q was 2×10^{-3} C, leading to n=3×10^{17} cm^{-2} and μ= 3×10^{-8} cm^2 V^{-1} s^{-1}. For LTO+C, for the same sweeping rate, again Q = 2×10^{-3} C and n= 3×10^{17} cm^{-2}, but in this case μ= 2×10^{-4} cm^2 V^{-1} s^{-1}. In the LTO+C case, the mobility is that of the composite materials (LTO and carbon conductive additive), not LTO.

Electrochemical response of TiO_2 IGTs

We run cyclic voltammograms of TiO_2 in [EMIM][TFSI] without and with Li^+ in the range 0 V to -2.5 V *vs.* activated carbon (Fig. 3 (a) and (b)). Without Li^+ (Fig. 3 (a)), the cyclic voltammograms obtained at different sweeping rates show a similar behaviour, namely no clearly distinguishable oxidation/reduction signals. In presence of Li^+, voltametric currents are about three times higher than in absence of Li^+ and voltammograms show signals similar to those observed for LTO films (Fig. 2 (a)). One broad reduction signal is observable between -2 V and -2.5 V whereas two barely distinguishable oxidation signals, at -1.75 V and -1.25 V, are observable during the oxidation scan. The two oxidation signals are better resolved with the decrease of the scan rate. The presence of Li^+ improves the resolution of the voltammetric signals, because their presence is mainly associated to Li^+ intercalation in LTO (in absence of Li^+, [EMIM] can bring about surface-confined electrochemical doping and a low concentration of H^+ might be present in the ion gating medium considering the fact that [EMIM][TFSI] is a protic ionic liquid).[38–41]

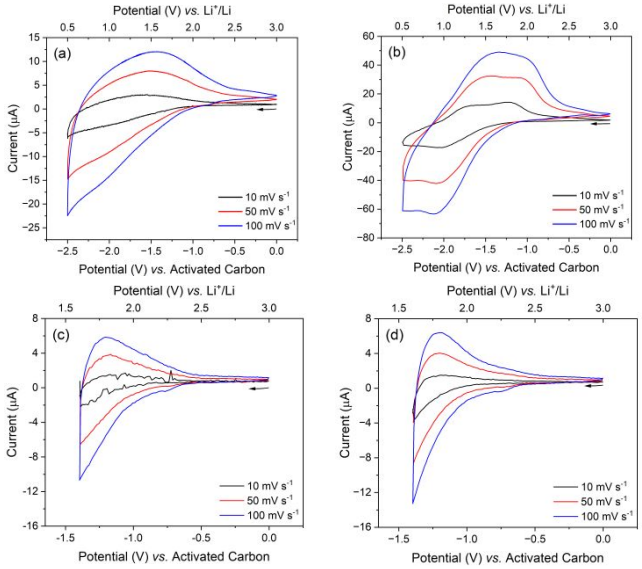

Fig. 3 Cyclic voltammograms of TiO_2 in IGT configuration at different sweep rates, potential windows and ion gating media. (a) and (c): [EMIM][TFSI]. (b) and (d) 0.1 mol L^{-1} LiTFSI in [EMIM][TFSI].

Fig. 3 (c, d) shows the cyclic voltammograms of TiO_2 without and with Li^+, in the range 0 V to -1.4 V vs activated carbon. The addition of Li^+ leads to a slightly higher cathodic current, as expected.[26]

Device characteristics of TiO_2 IGTs (V_{gs} from 0 V to 2.5 V)

The characteristics of TiO_2 IGTs upon application of V_{gs} values from 0 V to 2.5 V, in absence of Li^+ in the gating medium, show a typical n-type transistor behaviour (Fig. 4 (a,b) Fig. S6, Table S1). No clearly distinguishable peaks are observable in the I_{gs} plot (Fig. 4 (b)), in agreement with the voltammograms of Fig. 3 (a).

With Li^+ in the gating medium, the transistors still show a typical n-type behavior (Fig. 4(c)-(h), Table S1) but now I_{gs} plots show distinguishable signals (Fig. 4 (d), (f), (h)), in agreement with Fig. 3 (b), associated to the presence of electrochemical doping. In the V_{gs} range from 0 V to 2.5 V, without Li^+, at 10, 50, and 100 mV s^{-1}, the charge carrier densities were 5×10^{16} cm^{-2}, 2×10^{16} cm^{-2}, and 1×10^{16} cm^{-2} (Fig. S6). With Li^+, however, the values of *n* were 2.4×10^{17}, 1×10^{17} and 6.5×10^{16} cm^{-2}. In presence of Li^+, the values of *n* are higher than in absence of Li^+, due to a more advanced degree of electrochemical doping in the latter case. Further, the volumic charge carrier density (considering a film thickness of about 2.4 μm, see Experimental section) is $n=2\times10^{20}$ cm^{-3}, 8.5×10^{19} cm^{-3} and 6×10^{19} cm^{-3} in absence of Li^+, for V_{gs} scan rates of 10 mV s^{-1}, 50 mV s^{-1}, 100 mV s^{-1}, respectively. In presence of Li^+, the corresponding values are

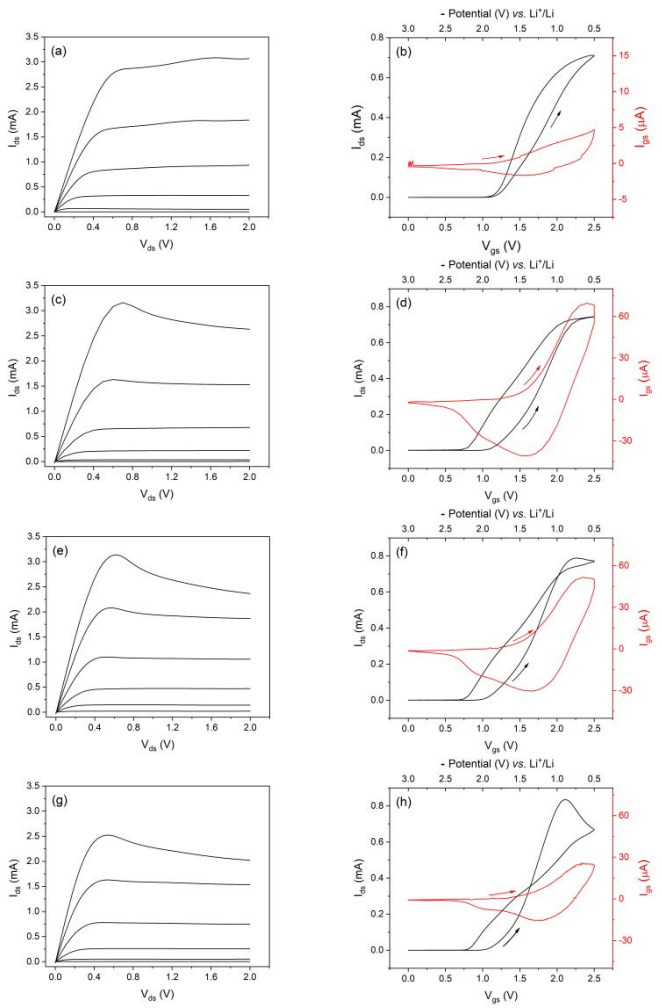

Fig. 4 TiO_2 IGTs with the ion gating medium [EMIM][TFSI]: (a) Output characteristics with V_{ds} at 10 mV s^{-1}; V_{gs} from 1 V to 2 V with 0.2 V steps. (b) Transfer characteristics with V_{gs} at 10 mV s^{-1}. V_{ds}= 0.1 V. Same type of transistors with ion gating medium 0.1 mol L^{-1} LiTFSI in [EMIM][TFSI]: (c), (d), (g) Output characteristics with V_{ds} at (c) 100, (e) 50, (g) 10 mV s^{-1}; V_{gs} from 1 V to 2 V with 0.2 V step. (d), (f), (h) Transfer characteristics with V_{gs} at (d) 100, (f) 50, (h) 10 mV s^{-1}, V_{ds}= 0.1 V.

9.9×10^{20}, 4.3×10^{20} and 2.7×10^{20} cm^{-3}. Such values of the volumic density have been associated in the literature to an insulator-metal Mott transition in the anatase form of titania.[42] The values of μ upon gating in in absence of Li^+ are 2×10^{-3}, 4.5×10^{-3}, and 6×10^{-3} cm^2 V^{-1} s^{-1} for V_{gs} sweeping rates of 10 mV s^{-1}, 50 mV s^{-1} and 100 mV s^{-1} whereas when Li^+ is present the corresponding values are 4×10^{-4} cm^2 V^{-1} s^{-1}, 1.2×10^{-3} cm^2 V^{-1} s^{-1} and 2×10^{-3} cm^2 V^{-1} s^{-1}.

In the presence of Li^+, for transfer curves obtained at 10 mV s^{-1}, we observe a decrease in the values of I_{ds} for V_{gs} above ca. 2.15 V. The shape of I_{gs} still indicates the presence of electrochemical doping. The presence of a maximum in the transfer curves could be explained by several contributions. Firstly, the Li^+ insertion process occurs through a first-order phase transition, from TiO_2 anatase to orthorhombic $Li_{0.5}TiO_2$.

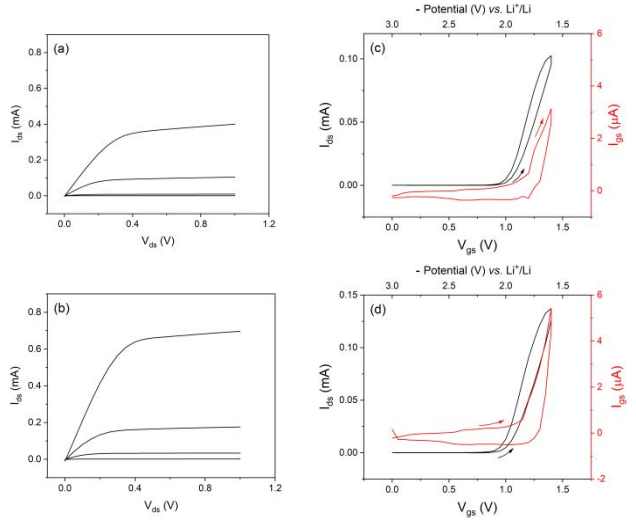

Fig. 5 TiO_2 IGTs. Output characteristics with V_{ds} at 50 mVs^{-1}, (a) [EMIM][TFSI], (b) 0.1 mol L^{-1} LiTFSI in [EMIM][TFSI], V_{gs} from 0.8 V to 1.4 V with 0.2 V steps. Transfer characteristics with V_{gs} sweep rate at 50 mV s^{-1}, V_{ds}= 0.1 V: (c) [EMIM][TFSI] and (d) 0.1 mol L^{-1} LiTFSI in [EMIM][TFSI].

Here, the conductivity is of about 0.4 S cm^{-1}, lower than that of Li-doped anatase TiO_2 (1.8 S cm^{-1}).[27] Secondly, the charge carrier density induced by the ion gating could high enough to bring about electron-electron screening effects, in turn causing a decrease of I_{ds}, analogously to what reported for organic IGTs, featuring finite windows of conductivity.[43,44] A further possibility to explain the decrease of I_{ds} could be that the proximity of Li^+ causes a decrease in the mobility of electrons and, hence, the electronic conductivity.

Device characteristics of TiO_2 IGTs (V_{gs} from 0 to 1.4 V)

TiO_2 IGTs were characterized in the V_{gs} range from 0 V to 1.4 V, a smaller interval with respect to the one already discussed. The aim of this study was to explore the early stages of the doping. The comparison of the transistor characteristics in absence (Fig. 5 (a), (c)) and presence (Fig. 5 (b), (d)) of Li^+ show slightly higher values of I_{ds} in the latter case.[39] No peaks are observable in the I_{gs} plots as expected for an electrostatic type of doping. Further, no maxima are observable in the transfer characteristics (different from results observed when values of V_{gs} probed are up to 2.5 V, as in Fig. 4).

Conclusions

In conclusion, we studied films of $Li_4Ti_5O_{12}$, both in pristine form (indicated as LTO) and as composite including a carbon conductive additive (indicated as LTO+C), and TiO_2 as channel materials in ion-gated transistors (IGTs), making use of the ionic liquid [EMIM][TFSI] including the salt LiTFSI. LTO+C and TiO_2 have been investigated in the literature as anode materials in Li-ion batteries (LIBs).

The IGTs characterized in this work behave as n-type transistors working in accumulation mode, under the action of a gate bias inducing the lithiation of the channel material.

We observed that for IGTs making use of pristine LTO (without carbon conductive additive) we need slow V_{gs} sweeping rates (1 mV s^{-1}) to observe a transistor behavior (not observable at 10, 50, 100 mV s^{-1}). For IGTs based on LTO+C films, a clear transistor behavior is observable at 1, 10, 50, 100 mV s^{-1}; a value of V_{ds}>0.1 V (e.g. 1 V) has to be applied, at all the mentioned sweeping rates, to make the electronic component of the current in the transistor clearly observable, with respect to the capacitive (ionic) component. For TiO_2, several doping mechanisms are possible, including the electrostatic (observable for low values of V_{gs}, between 0 V and 1.4 V), "purely" electrochemical (bringing about values of the charge carrier density typical of insulator-to-metal Mott transitions in anatase TiO_2) and, for values of V_{gs}>2.15 V and low V_{gs} sweeping rates (10 mV s^{-1}) an electrochemical mechanism where the increased concentration of Li^+ induces the formation of low-conductivity crystalline phases, thus explaining the decrease of the transistor current. Actually, electron-electron screening effects, as those previously observed in organic IGTs, could also explain the decrease of the current at high charge carrier density (about 10^{20} cm^{-3}).

Work is in progress on two fronts, at least. The study of other metal oxides used as electrode materials in LIB to assess the potential of our IGT approach to study the evolution of the electronic properties of LIB electrode materials with the lithiation/delithiation. Further, on a more fundamental side, we are studying the structure of the electrical double layers at the ion gating/channel interface as they ultimately govern the doping process in IGTs.

Author Contributions

Conceptualization: F. Soavi, C. Santato; Data Curation: C. Santato. J. R. Herrera Garza, F. Soavi, S. Khaleel, L. Neres Chagas Da Silva, L. Camargo, M Barbosa; Investigation: J. R. Herrera Garza, R. Karimi Azari, L. Camargo; Methodology: F. Soavi. J.R. Herrera Garza, C. Santato; Funding acquisition: C. Santato, F Soavi, J. R. Herrera Garza; Resources: C. Santato; Supervision: C. Santato, F. Soavi; Writing-original draft: J. R. Herrera Garza; Writing, reviewing and editing: all authors.

Conflicts of interest

There are no conflicts to declare.

Acknowledgements

The authors are grateful to C. Clement and Y. Drolet for their technical assistance. R.H.G. is grateful to Conacyt, C.S. to NSERC (DG), and C.S. and F.S. to Institut de l'énergie Trottier, for financial support. L.P.C and L.C.S.N are grateful to the Emerging Leaders of Americas Program (ELAP), support of Global Affairs Canada, and Coordenação de Aperfeiçoamento de Pessoal de Nível Superior (CAPES – Brazil) (Edital 44/2022-PROPG). M.S.B. acknowledges the Air Force Office of Scientific Research (AFOSR/SOARD, USA) under award number FA9550-23-1-0575.

References

1 X. Bu, H. Xu, D. Shang, Y. Li, H. Lv and Q. Liu, *Adv. Intell. Syst.*, 2020, **2**, 2000156.

2 R. Karimi Azari, T. Lan and C. Santato, *J. Mater. Chem. C*, 2023, **11**, 8293–8299.

3 F. Poli, J. R. Herrera, T. Lan, P. Kumar, C. Santato and F. Soavi, *iScience*, 2023, **26**, 105888.

4 S. Wang, Y. Yang, Y. Dong, Z. Zhang and Z. Tang, *J. Adv. Ceram.*, 2019, **8**, 1–18.

5 C. P. Sandhya, B. John and C. Gouri, *Ionics (Kiel).*, 2014, **20**, 601–620.

6 T. Ohzuku, A. Ueda and N. Yamamoto, *J. Electrochem. Soc.*, 1995, **142**, 1431–1435.

7 E. Peled and S. Menkin, *J. Electrochem. Soc.*, 2017, **164**, A1703–A1719.

8 M. Ma, A. N. Mansour, J. K. Ko, G. H. Waller and C. E. Hendricks, *J. Electrochem. Soc.*, 2020, **167**, 110549.

9 D. Young, A. Ransil, R. Amin, Z. Li and Y.-M. Chiang, *Adv. Energy Mater.*, 2013, **3**, 1125–1129.

10 T. A. Assefa, A. F. Suzana, L. Wu, R. J. Koch, L. Li, W. Cha, R. J. Harder, E. S. Bozin, F. Wang and I. K. Robinson, *ACS Appl. Energy Mater.*, 2021, **4**, 111–118.

11 K. Mukai, T. Nonaka and T. Uyama, *Energy Storage Mater.*, 2022, **44**, 547–556.

12 M. Uhlemann, M. Madian, R. Leones, S. Oswald, S. Maletti, A. Eychmüller and D. Mikhailova, *ACS Appl. Mater. Interfaces*, 2020, **12**, 37227–37238.

13 W. Zhang, D.-H. Seo, T. Chen, L. Wu, M. Topsakal, Y. Zhu, D. Lu, G. Ceder and F. Wang, *Science (80-.).*, 2020, **367**, 1030–1034.

14 J. Gao, W. Yang, C. Fang, J. Liang, T. Cheng, P. Li, X. Guo, Y. Jung, Y. Wang and X. Dong, *J. Mater. Sci.*, 2021, **56**, 14505–14517.

15 Y. Nam, J. H. Lim, K. C. Ko and J. Y. Lee, *J. Mater. Chem. A*, 2019, **7**, 13833–13859.

16 J. S. Edge, S. O'Kane, R. Prosser, N. D. Kirkaldy, A. N. Patel, A. Hales, A. Ghosh, W. Ai, J. Chen, J. Yang, S. Li, M.-C. Pang, L. Bravo Diaz, A. Tomaszewska, M. W. Marzook, K. N. Radhakrishnan, H. Wang, Y. Patel, B. Wu and G. J. Offer, *Phys. Chem. Chem. Phys.*, 2021, **23**, 8200–8221.

17 C. H. Sun, X. H. Yang, J. S. Chen, Z. Li, X. W. Lou, C. Li, S. C. Smith, G. Q. (Max) Lu and H. G. Yang, *Chem. Commun.*, 2010, **46**, 6129.

18 S. Paul, M. A. Rahman, S. Bin Sharif, J.-H. Kim, S.-E.-T. Siddiqui and M. A. M. Hossain, *Nanomaterials*, 2022, **12**, 2034.

19 N. J. J. de Klerk, A. Vasileiadis, R. B. Smith, M. Z. Bazant and M. Wagemaker, *Phys. Rev. Mater.*, 2017, **1**, 025404.

20 S. R. Damkale, S. S. Arbuj, G. G. Umarji, S. B. Rane and B. B. Kale, *RSC Adv.*, 2021, **11**, 7587–7599.

21 Y. Hu, Y. Pan, Z. Wang, T. Lin, Y. Gao, B. Luo, H. Hu, F. Fan, G. Liu and L. Wang, *Nat. Commun.*, 2020, **11**, 2129.

22 X. Q. Pan, S. J. Kim, K. Zhang, J. R. Jokisaari, A. Kargar, D. Wang and G. W. Graham, *Microsc. Microanal.*, 2015, **21**, 1367–1368.

23 J. H. Richter, A. Henningsson, P. G. Karlsson, M. P. Andersson, P. Uvdal, H. Siegbahn and A. Sandell, *Phys. Rev. B*, 2005, **71**, 235418.

24 M. Wagemaker, D. Lützenkirchen-Hecht, A. A. van Well and R. Frahm, *J. Phys. Chem. B*, 2004, **108**, 12456–12464.

25 C. L. Olson, J. Nelson and M. S. Islam, *J. Phys. Chem. B*, 2006, **110**, 9995–10001.

26 A. Subramanian, B. George, S. R. Bobbara, I. Valitova, I. Ruggeri, F. Borghi, A. Podestà, P. Milani, F. Soavi, C. Santato and F. Cicoira, *AIP Adv.*, 2020, **10**, 065314.

27 R. van de Krol, A. Goossens and E. A. Meulenkamp, *J. Appl. Phys.*, 2001, **90**, 2235–2242.

28 S. Liang, X. Wang, Y.-J. Cheng, Y. Xia and P. Müller-Buschbaum, *Energy Storage Mater.*, 2022, **45**, 201–264.

29 A. Wahl and J. Augustynski, *J. Phys. Chem. B*, 1998, **102**, 7820–7828.

30 J. Sayago, F. Soavi, Y. Sivalingam, F. Cicoira and C. Santato, *J. Mater. Chem. C*, 2014, **2**, 5690–5694.

31 P. W. Ruch, D. Cericola, M. Hahn, R. Kötz and A. Wokaun, *J. Electroanal. Chem.*, 2009, **636**, 128–131.

32 A. Hagfeldt and M. Grätzel, *Acc. Chem. Res.*, 2000, **33**, 269–277.

33 P. Hartmann, D.-K. Lee, B. M. Smarsly and J. Janek, *ACS Nano*, 2010, **4**, 3147–3154.

34 Y. Wang, Y. Zhang, W.-J. Yang, S. Jiang, X. Hou, R. Guo, W. Liu, P. Huang, J. Lu, H. Gu and J. Xie, *J. Electrochem. Soc.*, 2019, **166**, A5014–A5018.

35 L. Zheng, X. Wang, Y. Xia, S. Xia, E. Metwalli, B. Qiu, Q. Ji, S. Yin, S. Xie, K. Fang, S. Liang, M. Wang, X. Zuo, Y. Xiao, Z. Liu, J. Zhu, P. Müller-Buschbaum and Y.-J. Cheng, *ACS Appl. Mater. Interfaces*, 2018, **10**, 2591–2602.

36 H. Yan, D. Zhang, Qilu, X. Duo and X. Sheng, *Ceram. Int.*, 2021, **47**, 5870–5895.

37 B. D. Paulsen and C. D. Frisbie, *J. Phys. Chem. C*, 2012, **116**, 3132–3141.

38 T. Ohzuku, T. Kodama and T. Hirai, *J. Power Sources*, 1985, **14**, 153–166.

39 H. Lindström, S. Södergren, A. Solbrand, H. Rensmo, J. Hjelm, A. Hagfeldt and S.-E. Lindquist, *J. Phys. Chem. B*, 1997, **101**, 7717–7722.

40 S. Moitzheim, S. De Gendt and P. M. Vereecken, *J. Electrochem. Soc.*, 2019, **166**, A1–A9.

41 X. Meng, F. Quenneville, F. Venne, E. Di Mauro, D. Işık, M. Barbosa, Y. Drolet, M. M. Natile, D. Rochefort, F. Soavi and C. Santato, *J. Phys. Chem. C*, 2015, **119**, 21732–21738.

42 N. Mott, *Metal-insulator transitions*, CRC Press, London, 2004.

43 T. Lan, F. Soavi, M. Marcaccio, P.-L. Brunner, J. Sayago and C. Santato, *Chem. Commun.*, 2018, **54**, 5490–5493.

44 M. J. Panzer and C. D. Frisbie, *J. Am. Chem. Soc.*, 2005, **127**,

6960–6961.